Ionics (2018) 24:3725–3731
https://doi.org/10.1007/s11581-018-2545-z

ORIGINAL PAPER

Effect of molybdenum on $Li_2Mn_4O_9$ for rechargeable lithium ion batteries

K K Shaji[1] · S Sharmila[1] · George Sushama[2] · B Janarthanan[1] · J Chandrasekaran[3]

Received: 31 May 2017 / Revised: 20 March 2018 / Accepted: 27 March 2018 / Published online: 27 May 2018

Abstract

$Li_2Mn_4O_9$ and molybdenum-doped $Li_2Mn_4O_9$ have been prepared by simple solid-state method. Molybdenum is used as a dopant since it is resistant to both corrosion and high-temperature creep deformation. The structural, morphological, and electrical performances of the samples have been analyzed. The material exhibits a cubic structure with the fd3m space group. Using EDAX, the chemical compositions of the samples have been identified. The dc electrical conductivity of the Mo-doped (LM2) sample is found to be increased to 7.44×10^{-6} S cm^{-1} at 393 K. The enhanced electrical property of the molybdenum-doped $Li_2Mn_4O_9$ reveals it as a feasible cathode material for rechargeable Li-ion batteries.

Keywords $Li_2Mn_4O_9$ · Mo-doped · Solid-state method · Electrical properties

Introduction

Rechargeable Li-ion battery is an excellent energy storage device for the mobile battery cells, automobiles, HEV, and many of the household and portable applications. The rechargeable batteries based on Li were invented in 1980 by "Sony Energetic" and used $LiCoO_2$ as a first cathode material. The first rechargeable rocking chair battery system was commercialized in 1991 [1]. Since $LiCoO_2$ has a layer rock salt structure, it provides a 2D array of edge sharing LiO_6 octahedral, favorable, and reversible extraction of Li [2]. Lithium manganese oxide materials like $LiMnO_2$, $LiMn_2O_4$, $Li_4Mn_5O_{12}$ and $Li_2Mn_4O_9$ remain the most suitable because of its low cost, less environmental impact, outstanding cyclic capability, high power, and large cell voltage [3]. $Li_2Mn_4O_9$ has attractive properties such as it is free from Jahn Teller distortion, contains only tetravalent manganese, and can be easily prepared at low temperature range of 400–500 °C. The material shows a high discharge capacity of 213 Ah/Kg for $Li_2Mn_4O_9$ [4].

A de Kock et al. [5] suggested that $Li_2Mn_4O_9$ exhibits voltage of 3.5 V against pure lithium. Its highly oxidizing nature limits its usefulness in the lithium cells. High surface area of 78 m^2 g^{-1} and small average particle sizes ~3 μm characterize $Li_2Mn_4O_9$ electrodes which pave the way for the good electrochemical activity of the electrodes. M.M Thackeray et al. [6] synthesized lithium manganese oxide spinel by $MnCO_3$, Li_2Co_3 at 400 °C. By neutron diffraction data, he identified the occupancy of the lithium at 8d tetrahedral site and manganese on the 16d octahedral site. M.M Thackeray and M.H Rossoue [7] explained the stoichiometric spinel $Li_2Mn_4O_9$ can be prepared in moderately low temperature less than 500 °C by performing the reaction under the presence of nitrogen. This has a commercial implication for the production of $LiMn_2O_4$ which was synthesized at high temperature about 750–800 °C.

Christian Masquelier et al. [8] presented an idea of creating lithium and manganese vacancies on substitution of lithium for manganese on the 16d octahedral sites which lead to a higher value of average oxidation state of manganese between

✉ K K Shaji
shajikk7@gmail.com

S Sharmila
sharmila.s@kahedu.edu.in

B Janarthanan
janarthanan.b@kahedu.edu.in

[1] Department of Physics, Karpagam Academy of Higher Education, Coimbatore, India

[2] Department of Chemistry, Avinashilingam Institute for Home Science and Higher Education for Women University, Coimbatore, India

[3] Department of Physics, Sri Ramakrishna Mission Vidhyala College of Arts and Science, Coimbatore, India

3.5^+ and 4^+. Reduction of Mn^{3+} ion concentration results in suppression of the Jahn Teller Distortion. He Tao and W.U Haoquing [9] reported new cation deficient spinel $Li_{2.1}Cr_{0.44}Mn_{3.74}O_9$. A good electrical performance has been achieved for the Cr-doped $Li_2Mn_4O_9$ cycled between 3.6 and 2 V. S. Choi et al. [10] used solution-based chemical synthesis to access the spinel $Li_2Mn_4O_9$ at low temperature. In an intermediate calcined temperature, the lithium-rich $Li_2Mn_4O_9$ is obtained but the presence of small amount of Mn_2O_3 as impurity is obtained at a temperature of 700 °C. When the sample calcined at the temperature of 400 °C, a reverse capacity of about 130 mAh/g in the range of 3.8–2 V with excellent cyclability could be achieved for the $Li_2Mn_4O_9$. Kirloy et al. [11] synthesized $Li_2Mn_4O_{8+z}$ using carbonate and getting maximum value for z as 0.88 which shows a good capacity retention and stability at 4.5–2.5 V. Robert Kostecki et al. [12] reported lithium manganese oxide film on a platinum substrate. The film exhibits a capacity in both the 3 and 4 V regions. Strobel et al. [13] suggested the double vacancy scheme for $Li_2Mn_4O_9$ prepared by low temperature via solid-state reaction.

Eventually, scope of the present work is to prepare $Li_2Mn_4O_9$ using solid-state method and replace Mo (0.25–0.5 mol) into Mn sites of $Li_2Mn_4O_9$ in order to enhance the electrical conductivity and hence to obtain a suitable cathode material for rechargeable Li-ion batteries. Molybdenum was selected as the dopant since it possesses variable oxidation states, non-toxic, and highly resistive to corrosion. It also prevents the formation of a continuous protective oxide layer, which further ceases the bulk oxidation of the metal. Solid-state method was preferred since it is simple and low cost. It does not require any organic additives which change its morphology.

Experimental method

Synthesis

Spinel $Li_2Mn_4O_9$ micro particles are synthesized by simple solid-state method. Stoichiometric quantities of LiOH. $2H_2O$, and MnO_2 are used as the starting precursors. The samples are pulverized and mixed using the mortar and pestle. The mixture is calcined at 700 °C for 7 h in muffle furnace and cooled down to the room temperature. The obtained powders are crushed and used for further studies. 0.25 and 0.5 mol of Mo-doped sample is prepared using MoO_3 as the starting precursor and follows the same method as $Li_2Mn_4O_9$.

The structural characterization is done by X-ray diffraction with an XPERT-PRO diffractometer using CuKα radiation. Morphological analysis is performed using SEM analysis and chemical composition by EDAX. At different temperatures (333, 353, 373, and 393 K), the electrical properties are studied by impedance analyzer HIOKI 3532 LCR HITESTER in the frequency range of 50 Hz to 50 kHz.

For the preparation of electrodes, the active material $Li_2Mn_{3.75}Mo_{0.25}O_9$ activated carbon along with polyvinylidene fluoride as binder was taken in the weight ratio of 80:10:10 with N-methyl-2-pyrrolidone (NMP) as the dispersing solvent to form uniform slurry. After mixing for 15 min, the slurry was coated on a copper plate and dried at 60 °C for an hour, followed by vacuum drying at 120 °C overnight. The CR2032 coin-type cell was assembled in a glove box under an inert atmosphere with pure lithium metal as an anode and prepared electrode as a cathode. A polypropylene microporous membrane was used as separator and non-aqueous electrolyte 1 M $LiPF_6$ in 1:1 ratio of ethylene carbonate and dimethyl carbonate. The fabricated coin cells were charged to 4.3 V and then discharged to 2 V vs Li/Li^+. The charge-discharge and cycle performance were carried out at a scan rate of 0.2 mV/s in VMP3 BioLogic Electrochemical Workstation.

Results and discussion

Structural and morphological analysis

X-ray diffraction pattern of $Li_2Mn_4O_9$ and Mo-doped $Li_2Mn_4O_9$ is given in the Fig. 1. The obtained peaks are well agreed with JCPDS value (88-1608) and also with earlier reports [14]. The obtained diffraction peaks at $2\theta =$ 18.8°, 26 °, 36.53 °, 44.6 °, 64.4 ° corresponding to (111), (311), (400), and (440) plane, respectively. All the diffraction peaks can be indexed to fd3m space group with the face-centered cubic spinel structure. Some distinctive diffraction peaks of the samples exhibit other than the

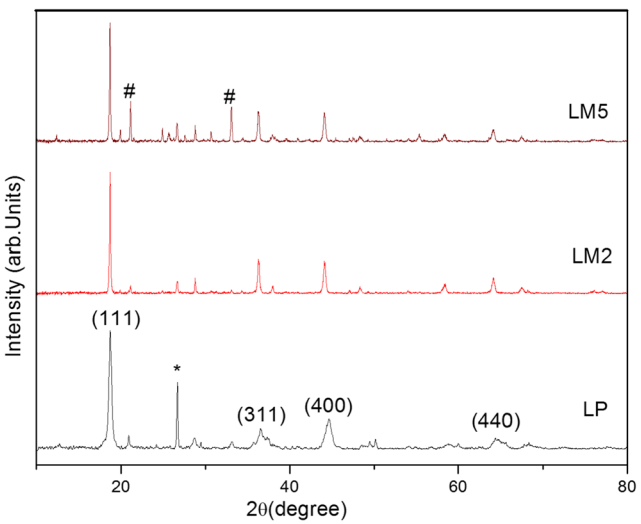

Fig. 1 XRD spectrum of LP) $Li_2Mn_4O_9$ LM2) $Li_2Mn_{3.75}Mo_{0.25}O_9$ LM5) $Li_2Mn_{3.5}Mo_{0.5}O_9$

Table 1 XRD parameters

Material	Lattice constant (Å)	Cell Volume (Å)^3	Lattice density (g cm^{-3})	Grain size (nm)
$Li_2Mn_4O_9$	8.164	544	24.35	41.6
$Li_2Mn_{3.75}Mo_{.25}O_9$	8.202	551	23.6	79.8
$Li_2Mn_{3.5}Mo_{0.5}O_9$	8.21	553	23.1	77.2

standard peaks at 2θ are 26° which was recognized as SiO_2 and also actualize from EDAX analysis. It is due to the lesser amount of impurities present in the precursors. Similarly, in Fig. 1, some additional peaks have been observed for LM2 and LM5 at 21.17 to 33.05 attributed to MoO_3 (89-1554 and 89-5108) representing some material may not enter into the lattice structure of $Li_2Mn_4O_9$. However, the intensity of (111) plane increases with the increasing concentration of the dopant. As per the structure of $Li_2Mn_4O_9$, the lithium ions in the Li-Mn-O phase must be located on the 8a sites. The transition elements dole out randomly on the 16d sites and oxygen on the 32 e sites [11]. The lattice parameter (a) is higher for Mo-doped $Li_2Mn_4O_9$ (8.216 Å) than pure $Li_2Mn_4O_9$ (8.16 Å). This effect is due to the substitution of Mo in Mn sites. The ionic radius of Mo (83 pm) is higher than Mn (72 pm). By increasing the concentration of the dopant, the lattice parameter also increases, which found to obey Vegard's law [15, 16]. The grain size of the molybdenum-doped $Li_2Mn_4O_9$ is higher comparing to pristine $Li_2Mn_4O_9$ due to the lattice expansion of the material (Table 1).

Figure 2 depicts the SEM images of pure and doped $Li_2Mn_4O_9$. The coral reef structure is reckoned for pristine sample. The pristine $Li_2Mn_4O_9$ exhibits the morphology of particles in micron size without any agglomeration. The doped material is found to be vivid with irregular morphology. The width of the particles ranges from 1 to 2 μm. Figure 3 shows compositional analysis of the prepared material. The presence of Mn, O, and Mo except lithium is confirmed from EDAX analysis.

Electrical analysis

In order to find the electrical conductivity of the materials, the complex impedance measurements are used.

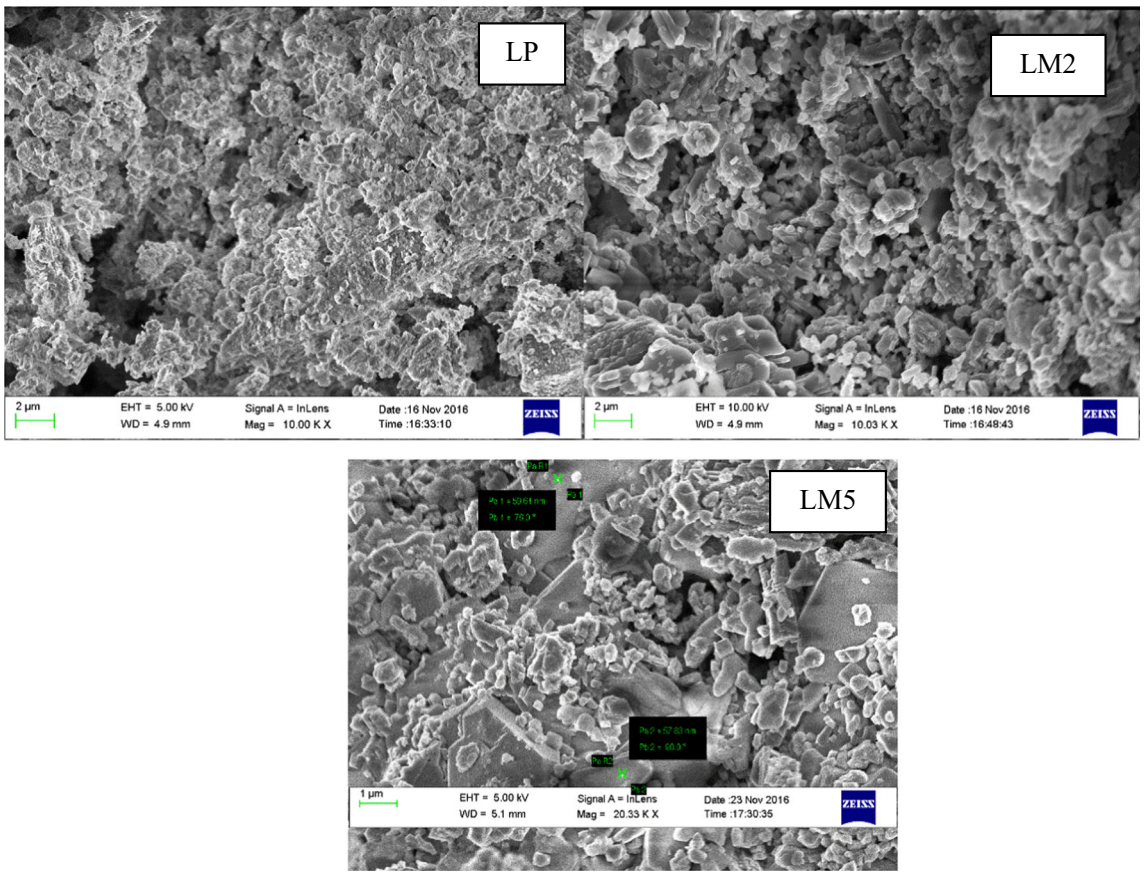

Fig. 2 SEM image of LP) $Li_2Mn_4O_9$, LM2) $Li_2Mn_{3.75}Mo_{0.25}O_9$, LM5) $Li_2Mn_{3.5}Mo_{0.5}O_9$

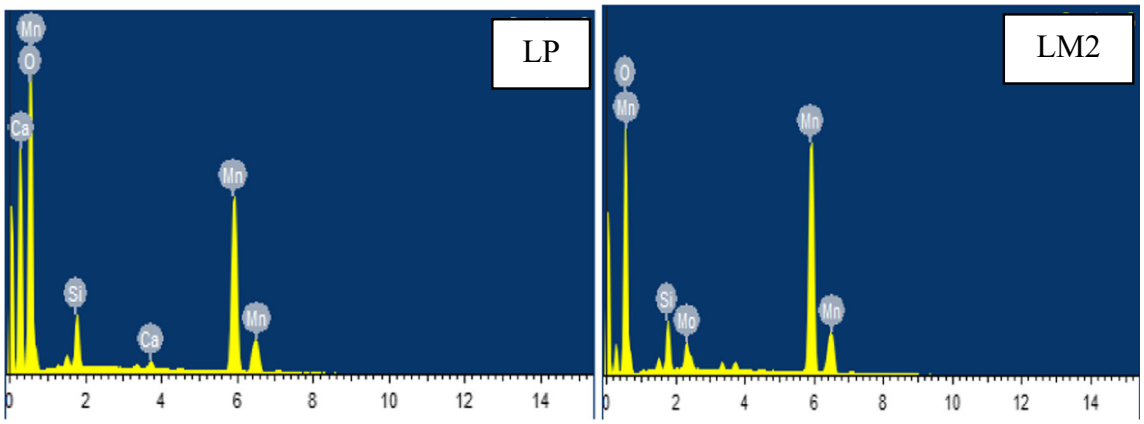

Fig. 3 EDAX analysis of LP) $Li_2Mn_4O_9$ LM2) $Li_2Mn_{3.75}Mo_{0.25}O_9$

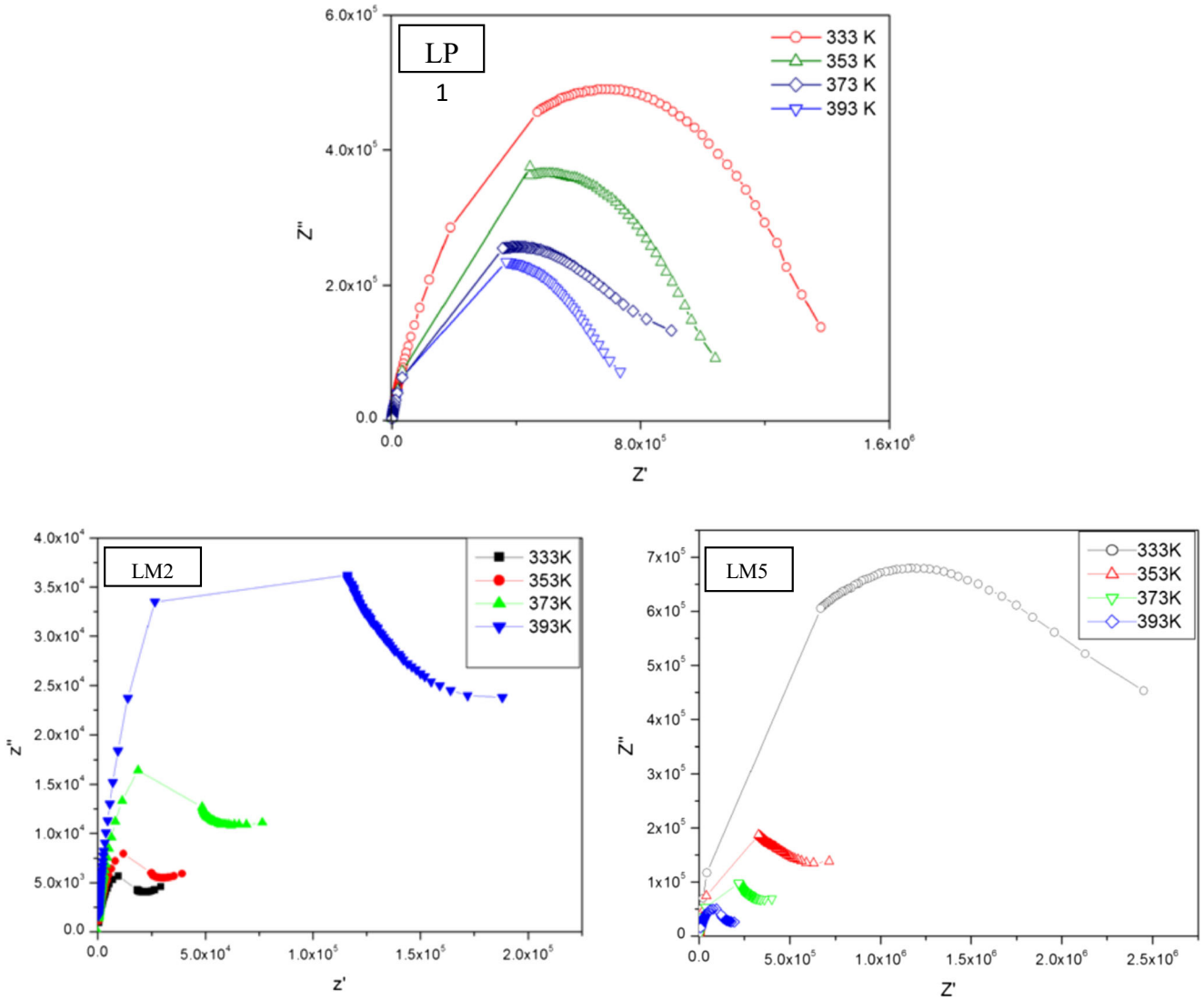

Fig. 4 Cole-cole plots of LP) $Li_2Mn_4O_9$, LM3) $Li_2Mn_{3.75}Mo_{0.25}O_9$ and LM5) $Li_2Mn_{3.5}Mo_{0.5}O_9$

Table 2. Electrical parameters

Material	Temp. (K)	$R_b \times 10^5\ \Omega$	C_b (pF)	$\sigma_{dc} \times 10^{-6}$ (S cm^{-1})	$\omega_p \times 10^4$ (Hz)	$N \times 10^{-9}$ (S cm^{-1} kHz^{-1})	$\mu \times 10^{20}$ (cm^2 V^{-1} s^{-1})	$D \times 10^{20}$ (cm^2 s^{-1})
L	333	13.8	38.7	0.105	0.30	10.75	0.60	1.8
	353	10.3	30.9	0.152	0.31	26.66	0.60	2.77
	373	8.94	3.56	0.171	0.92	10.84	1.61	1.38
	393	7.32	5.19	0.205	0.67	19.79	1.13	1.699
LM2	333	1.64	19.4	0.852	33.7	1.72	0.40	1.5
	353	0.607	52.4	2.36	11.52	1.36	1.6	6.77
	373	0.310	102.7	4.69	28.92	8.1	1.39	2.59
	393	0.196	162.4	7.44	22.85	1.5	2.2	3.2
LM5	333	21.3	44.8	0.0685	2.153	2.05	0.40	1.13
	353	6.22	51.2	0.242	9.27	1.65	1.6	6.8
	373	3.48	91.4	0.421	8.27	3.66	1.39	2.8
	393	1.72	61.1	0.835	13.93	2.4	2.22	5.6

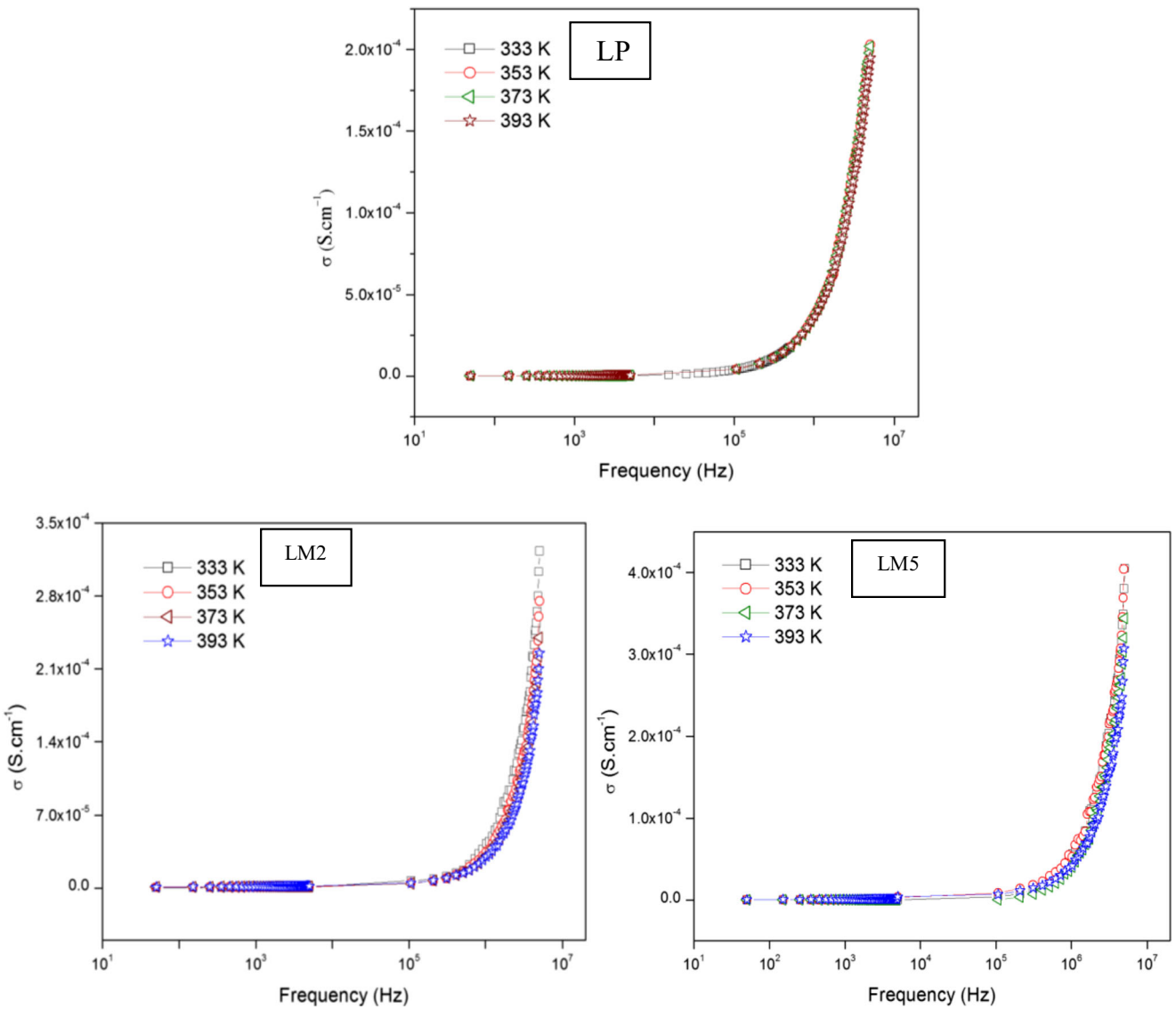

Fig. 5 Conductance spectra of LP) $Li_2Mn_4O_9$, LM2) $Li_2Mn_{3.75}Mo_{0.25}O_9$ and LM5) $Li_2Mn_{3.5}Mo_{0.5}O_9$

AC impedance feedback on the material is due to the combination of number of RC parallel cells. The impedance related to single R – C cell is Z = Z'-Z"

$$Z = \frac{R}{(1+\mathrm{Rc(t)})^2} - \mathrm{j}\frac{R(RC(t))}{(1+\mathrm{Rc}(t))^2}$$

where Z' and Z" are the real and imaginary part of Z.

The cole-cole plots of the pristine and doped materials are shown in Fig. 4 in the temperature ranging from 333 to 393 K. Due to the parallel combination of bulk resistance R_b and bulk capacitance C_b, the semicircle is formed in the high-frequency region for all the samples. It also indicates that the conduction is through the bulk of the material. In the low-frequency region, a small extension has been observed to indicate the presence of grain boundary effect. Migration of Li^+ ions at the electrode–electrolyte interface corresponds to the semicircle at high-frequency region. The bulk resistance decrease with increase in temperature indicates the semi-conducting nature, i.e., NTCR property of the material. The capacitance readings have been formulated for all the temperatures using the equation $2\pi\gamma_{max}R_bC_b = 1$ and given in Table 2. The capacitance values are found to be in the order of Pico farad and this shows the conduction process is through the bulk of the material [17]. The ionic conductivity of the material is estimated using the relation $\sigma = l/R_bA$ S cm^{-1}, where 'R_b' is the bulk resistance, 'l' the thickness, and 'A' area of the sample. It is found that the conductivity has been increasing with the increase in temperature due to the thermally activated mobile charge carriers.

Figure 5 shows the conductance spectra of pristine and doped $Li_2Mn_4O_9$. The measured frequency range of all the samples envisages two different conductance behaviors. The dispersive region at high-frequency region corresponds to σ_{ac} conductivity whereas the frequency-independent plateau at low-frequency region corresponds to σ_{dc} conductivity of the material. The conduction spectra found to obey the universal

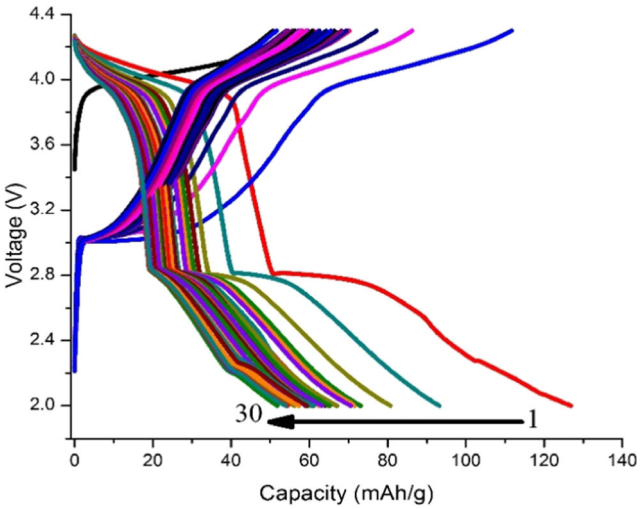

Fig. 6 Charge/discharge characteristics of $Li_2Mn_{3.75}Mo_{0.25}O_9$ cathode

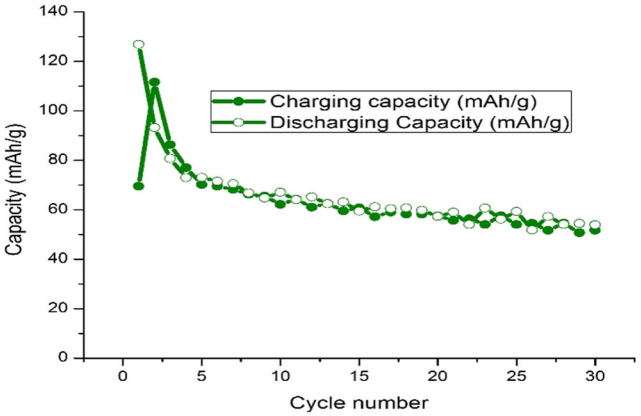

Fig. 7 Cycle life of $Li_2Mn_{3.75}Mo_{0.25}O_9$

Jonscher's law $\sigma(\omega) = \sigma_{dc} + A\omega^n$ [18]. The hopping frequency, charge carrier concentration, and mobility are calculated using the curve fitting method and presented in Table 2. High conductivity (7.44×10^{-6} S cm^{-1}) has been observed for $Li_2Mn_{3.75}Mo_{0.25}O_9$ at 393 K. The diffusion coefficient is found to be increasing with the temperature, envisage migration of more oxygen ions [19]. By increasing the concentration of dopant, the conducting values decreases, which may be due to the presence of some impurities as indicated in XRD spectrum, and the optimum concentration for molybdenum is 0.25 mol.

Electrochemical performance

Figure 6 shows the charge-discharge behavior of $Li_2Mn_{3.75}Mo_{0.25}O_9$ under galvanostatic conditions against lithium metal in 2032 coin cells. The fabricated cells were charged to 4.3 V and discharged to 2 V vs. Li/Li^+. Initially, the discharge capacity is measured as 128 mAh/g and gradually reduced to 52 mAh/g for the 30th cycle. According to S Choi et al. [10], when the temperature increases, the capacity reduces due to the crystalline formation of manganese oxide at low temperature and amorphous manganese oxide will shows high capacity. The present study also agrees with the earlier experimental results.

The cycling behavior of $Li_2Mn_{3.75}Mo_{0.25}O_9$ as cathode material was evaluated using $LiPF_6$ EC/DMC with potential window 4.3 to 2 V at 2C rate are shown in Figure 7. The initial discharge charge capacity is about 128 mAh/g and after the 10th cycle, it reduced to 70 mAh/g. By further increasing the cycle number, it again reduced to 52 mAh/g up to 30 cycles but 75% of capacity is retained.

Conclusion

Pure and Mo-doped $Li_2Mn_4O_9$ are successfully prepared by solid-state method. The structure and morphology of the

materials are examined using XRD, SEM, and EDAX analysis. The bulk resistance of the material is found to be decreased with the increase in temperature. It is least for 0.25 mol of Mo-doped $Li_2Mn_4O_9$ which shows the semiconducting property of the material. High conductivity of 7.44×10^{-6} S cm^{-1} is obtained at 393 K for $Li_2Mn_{3.75}Mo_{0.25}O_9$. The electrochemical tests of the cathode material exhibit a discharge capacity of 128 mAh/g, reduced to 70 mAh/g at 10 cycles and 75% of capacity retained at 30 cycles. Hence, $Li_2Mn_{3.75}Mo_{0.25}O_9$ is a feasible cathode material for the lithium-ion batteries.

Acknowledgements The author greatly acknowledges Dr. S.Gopakumar senior principal scientist, Lithium-ion battery division, CECRI, Karaikudi, Tamilnadu, India, for extending the cell fabrication and electrochemical investigation.

References

1. Mizushima K, Jones PC, Wiseman PJ, Goodenough JB (1980) Li_xCoO_2 (0<x<-1): A new cathode material for batteries of high energy density. Mater Res Bull 15(6):783–789
2. Guyomard D, Tarascon JM (1994) The carbon/$Li_{1+x}Mn_2O_4$ system. Solid State Ionics 69(3–4):222–237
3. Sharmila S, Janarthanan B, Chandrasekaran J (2016) Synthesis and characterization of Co-doped lithium manganese oxide as a cathode material for rechargeable Li-ion battery. Ionics 22:1567–1574
4. Barboux P, Tarascon JM, Shokoohi FK (1991) The use of acetates as precursors for the low-temperature synthesis of $LiMn_2O_4$ and $LiCoO_2$ intercalation compounds. J Solid State Chem 94(1):185–196
5. de Kock A, Rossouw MH, de Picciotto LA, Thackeray MM, David WIF, Ibberson RM (1990) Defect spinels in the system $Li_2O.yMnO_2$ (y>2.5): A neutron-diffraction study and electrochemical characterization of $Li_2Mn_4O_9$. Mater Res Bull 25(5):657–664
6. Thackeray MM, de Kock A, David WIF (1993) Synthesis and structural characterization of defect spinels in the lithium-manganese-oxide system. Mater Res Bull 28(10):1041–1049
7. Thackeray MM, Rossouw MH (1994) Synthesis of Lithium-Manganese-Oxide Spinels: A Study by Thermal Analysis. J Solid State Chem 113(2):441–443
8. Masquelier C, Tabuchi M, Ado K, Kanno R, Kobayashi Y, Maki Y, Nakamura O, Goodenough JB (1996) Chemical and Magnetic Characterization of Spinel Materials in the $LiMn_2O_4$–$Li_2Mn_4O_9$–$Li_4Mn_5O_{12}$System. J Solid State Chem 123(2):255–266
9. He T, Wu H (1999) Characterization of a new spinel Li–Cr–Mn–O for secondary lithium batteries. J Electroanal Chem 463(1):24–28
10. Choi S, Manthiram A (2000) Synthesis and Electrode Properties of Metastable $Li_2Mn_4O_{9-\delta}$ Spinel Oxides. J Electrochem Soc 147(5):1623–1629
11. Kilroy WP, Ferrando WA, Dallek S (2001) Synthesis and characterization of $Li_2Mn_4O_9$ cathode material. J Power Sources 97–98: 336–343
12. Kostecki R, Kong F, Matsuo Y, Larnon FM (1999) Interfacial studies of a thin-film $Li_2Mn_4O_9$ electrode. Electrochim Acta 45(1–2): 225–233
13. Strobel P, Ibarra A, Anne PM (2001) $Li_2Mn_4O_9$ revisited: crystallographic and electrochemical studies. J Power Sources 97–98: 381–384
14. Hao YJ, Lai QY, Wang L, Xu X-Y, Chu HY (2010) Electrochemical performance of a high cation-deficiency $Li_2Mn_4O_9$/active carbon supercapacitor in $LiNO_3$ electrolyte. Synth Met 160:669–674
15. Nithya VD, Sharmila S, Vediappan K, Lee CW, Vasylechko L, Kalai Selvan R (2014) Electrical and electrochemical properties of molten-salt-synthesized 0.05 mol Zr- and Si-doped $Li_4Ti_5O_{12}$ microcrystals. J Appl Electrochem 44:647–654
16. Shenouda AY, Murali KR (2008) Electrochemical properties of doped lithium titanate compounds and their performance in lithium rechargeable batteries. J Power Sources 176(1):332–339
17. Jonscher AK (1977) The 'universal' dielectric response. Nature 267:673–679
18. Nithya VD, Kalai Selvan R, Vediappan K, Sharmila S, Lee CW (2012) Molten salt synthesis and characterization of $Li_4Ti_{5-x}Mn_xO_{12}$ (x = 0.0, 0.05 and 0.1) as anodes for Li-ion batteries. Appl Surf Sci 261:515–519
19. Nithya VD, Kalai Selvan R (2011) Synthesis, electrical and dielectric properties of $FeVO_4$ nanoparticles. Phys B Condens Matter 406(1):24–29